# Simulation of Laser Shock Peening on X12Cr Steel Using an Alternate Computational Mechanical Threshold Stress Plasticity Model

Festus FAMESO [a]*, Dawood DESAI [a], Schalk KOK [b], Mark NEWBY [c], and Daniel GLASER [d]

[a] Department of Mechanical and Automation Engineering, Tshwane University of Technology, Pretoria, South Africa.

[b] Department of Mechanical and Aeronautical Engineering, University of Pretoria, Pretoria, South Africa.

[c] Eskom Holdings SOC Ltd, Johannesburg, South Africa.

[d] CSIR National Laser Centre, Brummeria, Pretoria, South Africa.

*Corresponding Author: festus.fameso@gmail.com

**ABSTRACT** – The ever-increasing relationship between energy consumption and economic growth continues to reinforce functional power generation infrastructure as the centre piece of development. However, downtimes from in-service failure of power plant components, such as turbine blades, portends dire consequences in the form of huge financial and safety concerns. This challenge is now being progressively overcome through intensive research in the development of laser shock peening (LSP) models, which simulate the induction of compressive layers around and beneath the surface of the blades. This paper presents an alternate experimentally validated computational modelling approach of the LSP process, grounded on a physics-based plasticity model which describes a mechanical threshold for compressive residual stress induction irrespective of increasing laser shock intensities. This is a phenomenon which hitherto has previously been overlooked by many researches. The results of this work show considerable promise when compared to experimental results.

Keywords: Compressive residual stresses, Laser shock peening, Mechanical threshold, Turbine blades

## 1. INTRODUCTION

Energy generation is at the heart of contemporary global economic development, as well as future technological growth and prosperity projections. Current indices indicate continued reinforced heightening of the interrelationships between energy and economy, however, progressive increases in population, over and above, has gate-crashed this loop. According to [1], between 15 to 20 % increase in global population demographics is expected by the middle of the century, and with-it rising demand for energy as a result of income, consumption and energy application trends. With the growing demand for digital connected devices and electrification of transport and heat, and air conditioning in response to environmental challenges, the nature of energy demand and consumption globally, requiring uninterrupted supply of energy to an increasingly fast paced global economy has made provision of adequate quantum of energy to consumers become an increasingly primordial imperative for many governments at all levels.

In the face of rising demand, yet with no proportional increase in hardware capacity, power generating companies are expected to meet the supply gaps to balance the global annual 2.1% electricity demand increase [2]. Turbines are at the heart of energy/power generation plants, often stretched to their limits to sustain electricity output requirements governed by the demands of consumers. Operating in highly stressed environments where hydraulic flow and centrifugal forces generate high stresses on them, the

process of design, manufacture and maintenance of turbine parts, especially the blades, usually involves paying intricate attention to factors such as temperature, hydrodynamic forces, and/or the metallurgical limits of the fabrication material. All which are necessary to enable the unit function safely and optimally in service. Even so, they are still subject to suffering greatly resulting in bending, fretting, developing cracks - usually at the surfaces, fatigue and eventual failure. [3] showed in his study that low pressure steam turbine blades are generally more susceptible to failure than those of the high pressure and intermediate pressure, with almost 50% of their failures being related to any of, or a combination of fatigue, stress corrosion cracking, and corrosion fatigue.

Laser shock peening (LSP) has evolved from an object of laboratory curiosity to a technique which has recently found novelty in industrial applications to mitigate the initiation and effects of failure mechanisms on turbine blades. Researchers and engineers have developed the technique to improve the surface and microscopic properties of materials in a bid to help them withstand these rather harsh conditions, improve fatigue resistance and extend their useful live. LSP uses high-powered lasers reaching gigawatts per square centimetre in magnitude of intensity to induce compressive residual stresses (CRS) in the top layer of the surface of blade to delay initiation of cracks, retard its propagation and improve its resistance to fatigue or failure by erosion or fracture. Laser shock peening it involves the firing of high intensity laser pulses onto a water confined opaque ablative layer applied to the target material, causing plasma formation on the surface. This plasma formation is occasioned by the instantaneous vaporisation of the atomic layers of the ablative material, driving shock waves propagated by the interaction into the underlaying metal. The high-pressure expanding plasma is often amplified by the presence of the confining layer which traps it, re-directs it into the material and sustain it throughout the duration of the shock impaction till its eventual dissipation. Subsequently, compressive residual stresses remain in the part, improving damage tolerance, fatigue strength and ultimately, the useful life of the material. For far reaching effects, it is common in practice to laser-peen the part at different spots and/or at intervals as it is moved around, repeating the sequence at each of these spots [4]. Studies have since shown that LSP provides better CRS penetration in depth compared to other surface treatments, also providing resistance to corrosion, wear and damage due to foreign objects impact [5].

The development of advanced numerical and computational capacities in the last decade or two has opened up prospects for research into laser shock processing, especially in applications ranging from manufacturing, condition-based maintenance and engineering processes; finding applicability in the global power, energy, automotive, aviation and aerospace industries, with many committing huge resources to its integration. Employing commercial finite elements analysis (FEA) modelling and simulating software, [6] successfully pioneered attempts at modelling LSP with computers. Overtime, especially in the two decades that followed the success of computer simulation of LSP, [7 – 13] amongst others, have also employed computer simulations to carry out various studies on various parameters of LSP. In line with development needs and the fast-paced nature of industry operations, there is also growing research efforts at developing simulation methodologies which are time efficient and provide reliable results. This is being done to provide competitive edge for incorporating the LSP technology into industry condition-based maintenance operations.

As important as the simulation steps are to the accuracy of results obtainable from an analysis, so are the constitutive models adopted in defining the physics of the problem before analysis. Contemporary methodologies are mostly interpolatory, physically inconsistent hence lacking in requisite predictive capabilities as noted by [13] in his editorial, and as such do not extensively describe stress saturation, which may be responsible for internal ruptures due to over processing discovered in a study carried out by [14]. However, this paper presents an alternate computational modelling of the LSP process,

grounded on a physics-based plasticity model which describes a mechanical threshold for compressive residual stress induction irrespective of increasing shock intensities. The mechanical threshold stress (MTS) model is a non-empirical, fully physics-based material model, which demonstrates plasticity behaviour with full path dependency on state variable evolution [15]. This is a phenomenon which hitherto has previously been overlooked by many researchers, but is increasingly becoming important, as the LSP process continues to find application in industry. The results of the study, which are very promising, have been validated experimentally.

## 2. LSP ANALYSIS BY FINITE ELEMENT (FE) SIMULATION

Solving analytically the complex physics of collisions, elasto-plastic deformations and wave propagation which are microphysical manifestations of impinging high pressure laser pulses on engineering materials has since been replaced with less cumbrous and more efficient numerical solutions obtained from finite element models and simulations, thanks to the development and emergence of advance electronic computation devices and programs. This has also provided more avenues and a broader research space for the exploration and discovery of novel methods and techniques for laser shock peening process of materials.

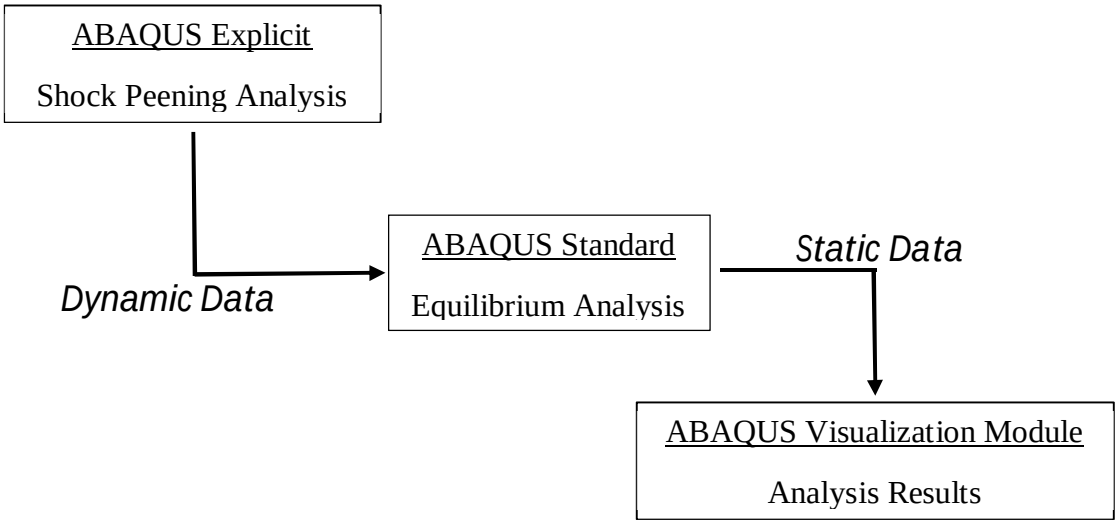


Figure 1: The Conventional LSP explicit-implicit simulation approach [6]

Conventionally, FEM techniques for LSP research have presented and applied the coalescence of two finite element commercial codes, ABAQUS/Explicit and ABAQUS/Standard, in a method often referred to as explicit-implicit FE modelling of LSP. As described in Figure 1, The first step simulates the pressure pulse temporal profile generated from the laser pulse, followed by the plastic deformation of the target material. The results of this process feeds as a pre-defined input into the second step calculates relaxation of the dynamic effects in the component to the point where eventually, static equilibrium is achieved, providing overall output results which are in good equivalence with experiments. However, shortfalls revolving around computational time and space management, taking cognisance of the simulation duration and the cost of computation, especially for multiple laser shocks, called for further development of techniques such as the coupled explicit-damping technique employed in this study.

The coupled explicit-damping method as illustrated in Figure 2 incorporates both the dynamic processes as well as the timed damping of the propagated stress waves to saturation point in a single finite element analysis. Additional damping, aided by the application of viscous pressure to the shock surface in successive relaxation steps succeeding a loading steps, contributes to the damping out dynamic effects to quasi-static condition which is equivalent to the kinetic energy being near zero and reaching equilibrium in fewer increments, thus eliminating the need to invoke implicit algorithm to obtain the final residual stress profiles in static equilibrium. This achieved a faster equilibrium in residual stress results there by addressing the constraints of computational cost and time.

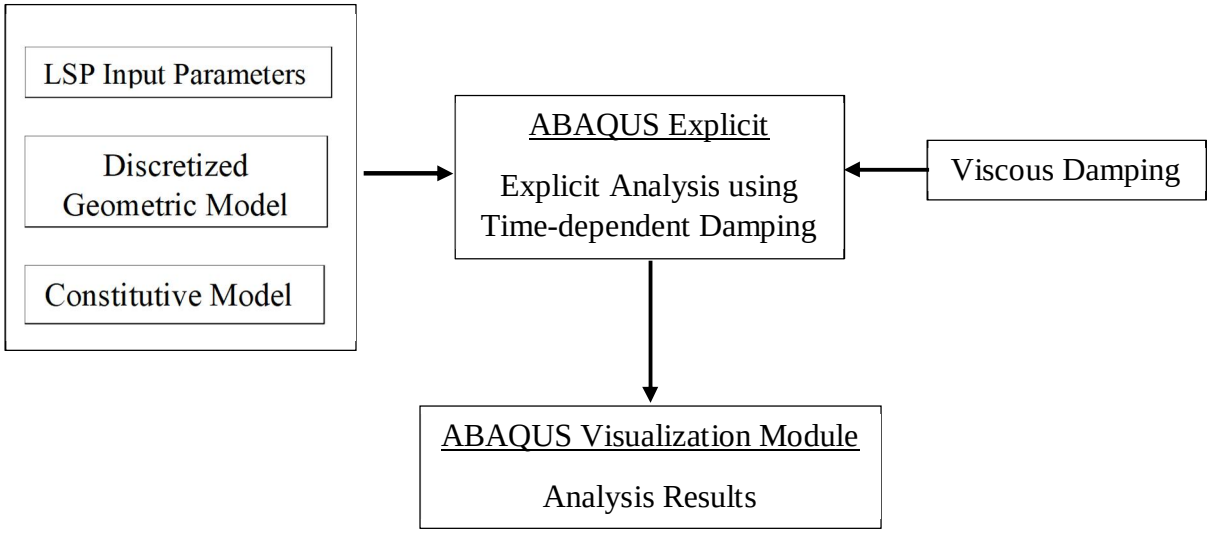


Figure 2: The coupled explicit-damping simulation procedure

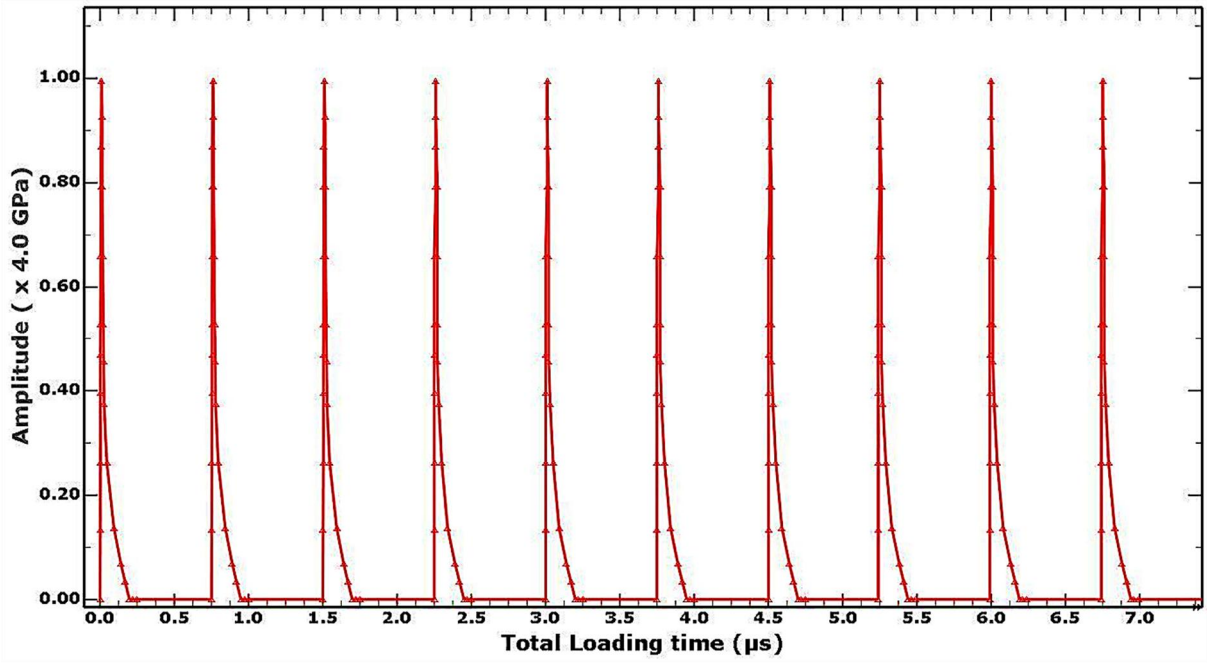


Figure 3: Laser shock loading pulse profile for sequence of explicit-damped steps

An integral algorithm is used to explicitly solve the set of nonlinear equations for each crystal. The analysis also uses a novel state variable integration method which renders the analysis time step size independent for constant strain rate simulations [16]. As illustrated in Figure 3, in the first step, loading is applied while the second step, which is a no-load step, involves the wave propagation in material, with the step time being a few orders of magnitude longer than the first, and being enough to bring the system close enough to equilibrium. A state of equilibrium can be achieved once the system kinetic energy damps down to 1% of maximum kinetic energy [17]. This is further assisted by implementing infinite boundary elements in the mesh element type selection as with an advancing front meshing format. An extended final explicit damping step period is introduced after defining all the successive sequences of the laser shots to de-excite the model to quasi-static equilibrium. This variable damping ensures a significant reduction of computation costs and time.

## 3. MATERIAL AND CONSTITUTIVE MODEL

The primary components of all polycrystal models are the constitutive behaviour of single crystals and a mean field hypothesis which delivers the macroscopic response, given the individual crystal response [17]. The fidelity of LSP structural-response predictions of the MTS model relies heavily on the constitutive model's accuracy in describing a plasticity threshold in the form of the individual crystal response to shock plasma propagation with respect to the macroscopic polycrystal response to strain-hardening induced dislocation accumulation and annihilation. The model is developed based on two principal concepts i.e. flow stress in the presence, and in the absence of thermally activated microstructural processes, such as dislocation motion and interaction as well as microstructural evolution, during laser shock induced deformation. The material flow stress formulation, decomposed to reflect a thermal and athermal component, is given by Equation 1 [18]:

$$\sigma_y\left(\epsilon_p, \dot{\epsilon}_p, T\right) = \sigma_a + \sum_k \sigma_t^k \tag{1}$$

$\sigma_y$, $\sigma_a$, and $\sum_k \sigma_t^k$ representing the flow stress, athermal and thermal component of the model respectively. $\epsilon_p$ and $\dot{\epsilon}_p$ are the plastic strain and strain rates respectively. The thermal component is expanded further in Equation 2 [19] as:

$$\sum_k \sigma_t^k = \left(S_i \sigma_i + S_e \sigma_e\right) \frac{\mu(T)}{\mu_0} \tag{2}$$

where, $\sigma_i$ is the intrinsic component of flow strain due to barriers to thermally activated dislocation motion. $\sigma_e$ is the strain hardening component of the flow stress, $S_i$, $S_e$, $\mu$, and $\mu_0$ are strain rate and temperature dependent scaling factors, Shear modulus and Shear modulus at 0 K respectively. Thermo-physical effects are incorporated into the MTS strength model framework by a temperature and strain-rate dependent scaling factor $S$, obtained by Equation 3 [19];

$$\mathrm{S} = \left(1 - \left(\frac{\mathrm{kT}}{\mathrm{g_0 \mu b^3}} \ln \frac{\dot{\epsilon}_0}{\dot{\epsilon}}\right)^{\frac{1}{\mathrm{q}}}\right)^{\frac{1}{\mathrm{p}}} \tag{3a}$$

Thus: $S_i = \left(1 - \left(\frac{\mathrm{kT}}{\mathrm{g_{0i} \mu b^3}} \ln \frac{\dot{\epsilon}_0}{\dot{\epsilon}}\right)^{\frac{1}{q_i}}\right)^{\frac{1}{p_i}}$ and $S_e = \left(1 - \left(\frac{\mathrm{kT}}{\mathrm{g_{0e} \mu b^3}} \ln \frac{\dot{\epsilon}_0}{\dot{\epsilon}}\right)^{\frac{1}{q_e}}\right)^{\frac{1}{p_e}}$ (3b)

where T is the reference temperature, k is Boltzmann's constant, b represents Burgers vector and p, q are empirical constants. Thus, the equivalent flow stress comes together as;

$$\sigma_y = \sigma_a + S_i(\dot{\epsilon}_p, T)\sigma_i \frac{\mu(T)}{\mu_0} + S_e(\dot{\epsilon}_p, T)\sigma_e \frac{\mu(T)}{\mu_0} \tag{4}$$

The instantaneous temperature dependent shear modulus $\mu(T)$ is expressed as;

$$\mu(T) = \mu_0 - \frac{D_0}{\exp\frac{T_0}{T} - 1} \quad (5)$$

With the stage-wise evolution of the strain hardening component of the flow stress $\sigma_e$ to a temperature and rate dependent threshold stress is given by [20] as the modified Voce-law;

$$\frac{d\sigma_e}{d\epsilon_p} = \theta_0 \left(1 - \frac{\sigma_e}{\sigma_s}\right)^{\alpha} \quad (6)$$

Hence the saturation threshold stress as a function of the strain rate and temperature reduces to

$$\sigma_s = \frac{\sigma_{s0}}{\exp\left(\frac{a_{e0}\mu}{T}\right)} \left(\frac{\dot{\epsilon}_p}{\dot{\epsilon}_{s0}}\right) \quad (7)$$

Where $\theta_0$ is the initial hardening rate and $D_0, T_0, \sigma_{s0}, a_{e0}, \dot{\epsilon}_{s0}$ are the nominal shear modulus, nominal temperature, reference saturation stress, activation energy and strain rate for dislocation accumulation or annihilation. The stress propagation and deposition response of the peened material is well characterized by the MTS scheme in which the temperature and strain-rate sensitivities of the yield strength and strain hardening is described by a single expression, therefore requiring a single set of parameters to describe the microstructural evolution once the induced shock wave proceeds into the peened material. This implies that, unlike empirical models where re-calibration of parameters and interpolation over a range of strain rates are necessary to obtain results for the ultra-high strain rate of $10^6 s^{-1}$ in which laser shock peening occurs, induced residual stress prediction using the MTS constitutive model provides first principle analysis, thereby eliminating analysis errors due to approximations and rounding and as such provides a closer degree of accuracy. The chemical composition, material mechanical properties and constitutive model parameters for the X12Cr steel under investigation in this study are respectively provided in Tables 1 – 2.

Table 1: Chemical Composition of X12Cr Steel [21]

| Element | C | Si | Mn | Ni | P | S | Cr | Mo | V |
|---|---|---|---|---|---|---|---|---|---|
| Percentage Composition | 0.08 – 0.15 | Max 0.35 | 0.50 – 0.90 | 2.0 – 3.0 | Max 0.025 | Max 0.020 | 11 – 12.5 | 1.5 – 2.0 | 0.25 – 0.40 |

Table 2: Mechanical Properties of X12Cr Steel [21]

| Density ($kg/m^3$) | Young's Modulus (GPa) | Poisson's Ratio | Yield Stress (MPa) | Ultimate Tensile Stress (MPa) | Elastic Limit (MPa) | Elongation (%) | Melting Temperature (K) |
|---|---|---|---|---|---|---|---|
| 7 700 | 204 | 0.3 | 870 | 1 145 | 275 | 20 | 1 793 |

Table 3 provides the MTS model parameters for the material, obtained from Gleeble experiments on samples cut out from out-of-service steam turbine blades, subjected to Gleeble presses and processed into force vs corresponding displacement curves at constant strain rate and varied temperatures, and then at constant temperature and varied strain rates successively. The model parameters obtained were thereafter subjected to further optimization using a Pareto frontier to correctly fit the parameters onto the strain rates occurring in during a typical LSP process.

Table 3: Optimized MTS Model Parameters for X12Cr Steel [22]

| Parameter | Value |
|---|---|
| Shear Modulus at 0 K($\boldsymbol{\mu_0}$) | 71 GPa |
| Nominal Shear Modulus ($\boldsymbol{D_0}$) | 8.64 GPa |
| Nominal Temperature ($\boldsymbol{T_0}$) | 208 K |
| Athermal Yield Stress Component ($\boldsymbol{\sigma_a}$) | 0 MPa |
| Saturation Threshold Stress for Deformation at 0 K ($\boldsymbol{\sigma_{so}}$) | 1.77 GPa |
| Intrinsic Stress Component ($\boldsymbol{\sigma_i}$) | 2.193 GPa |
| Initial Hardening Rate ($\boldsymbol{\theta_0}$) | 9.18 GPa |
| Reference Maximum Strain rate ($\boldsymbol{\epsilon_{so}}$) | $10^7$ |
| Inter-crystal Structural evolution parameters ($\boldsymbol{q_e}$, $\boldsymbol{p_e}$) | 1, 2/3 |
| Inter-crystal Glide-Obstacle Profile Parameters ($\boldsymbol{q_i}$, $\boldsymbol{p_i}$) | 3/2, ½ |

This constitutive model was specially coded as a VUHARD user-defined Fortran subroutine for implementation in the primary numerical FE code to acquire derivatives of the flow stress ie the flow stress itself, the flow stress differential with respect to temperature as well as the flow stress differential with respect to strain rate at different states, based on the stage-wise hardening evolution, which are defined as functions of the plastic strains, temperature and the strain rates. The subroutine was implemented by the transformation of the rate and temperature dependent yield stresses into increments which are returned as new state variables for every increment in the explicit solver which employs a forward integral analysis method. Figure 4 synopsizes the implementation of the VUHARD subroutine in the Abaqus Explicit ® FEA tool.

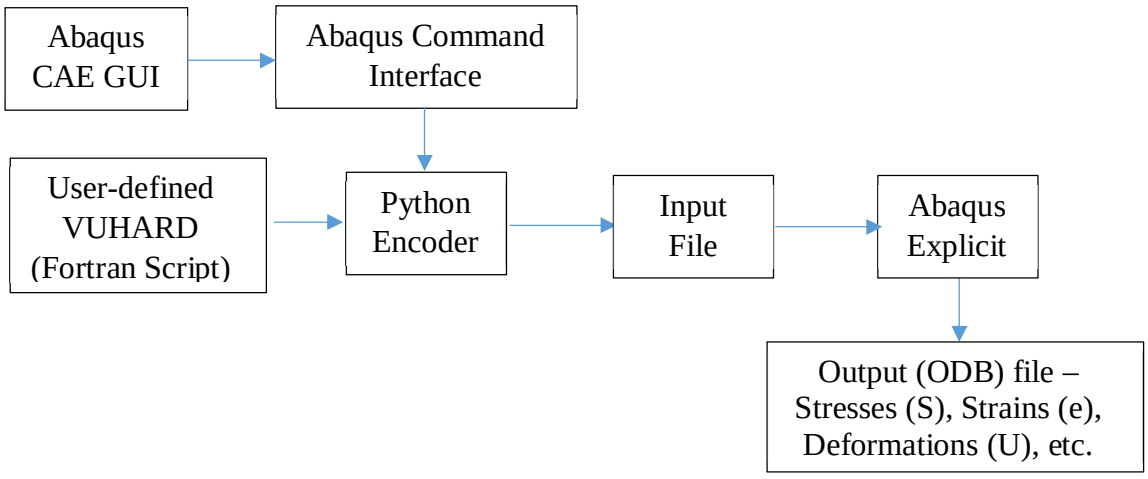


Figure 4: VUHARD User-Subroutine Implementation in Abaqus Explicit

## 4. FINITE ELEMENT ANALYSIS

### *4.1 Pressure loading*

With a high power laser directed at a particular location or target on the part, and the subsequent pressure pulse generated, only existing for a nanoscale duration, the effectual quantum of laser shock on the peened workpiece is defined by a measured relationship and interdependence between the magnitude of the laser power, the temporal and the spatial profiles of the laser beam, reaching a peak somewhere in between. This can be at angles between tangential ($90^o$) and normal ($0^o$) to the part. To simulate the LSP processes, these interrelationships and interdependence where specified in the python script of the input file as real number magnitudes obtained by Equation 7 [12].

$$P_{max} = 0.01 \sqrt{\frac{\alpha}{2\alpha+3}} \cdot \sqrt{\frac{2Z_1Z_2}{Z_1+Z_2}} \cdot \sqrt{I_o} \tag{7}$$

which eventually reduces to Equation 8 [10];

$$P_{max} = 1.65 \sqrt{I_o} \tag{8}$$

Where $P$, is the magnitude in gigapascals of the pressure pulse generated by a laser of gigawatts per square centimetre power intensity, $Z_1$ and $Z_2$ are the impedances in pascal-seconds per cubic meter offered by the peened material and the confining layer respectively. The pressure pulse is delineated by the short rise time temporal profile defined by the pressure-space-time relationship of the generation of pressure pulse from bursting of plasma given in Equation 9 [12], expounding the spatial-temporal laser beam profile between the beginning and the end of the loading phase.

$$P(r,t) = P_{max} \cdot P(t) \cdot exp\left(\frac{-r^2}{2R^2}\right) \tag{9}$$

where r is the radial distance from the centre of laser spot and R is the laser spot radius. Figure 5 shows the time dependent profile of the laser pulse $P = f(t)$ for a 20 ns width at half maximum used in the simulation as obtained from [23].

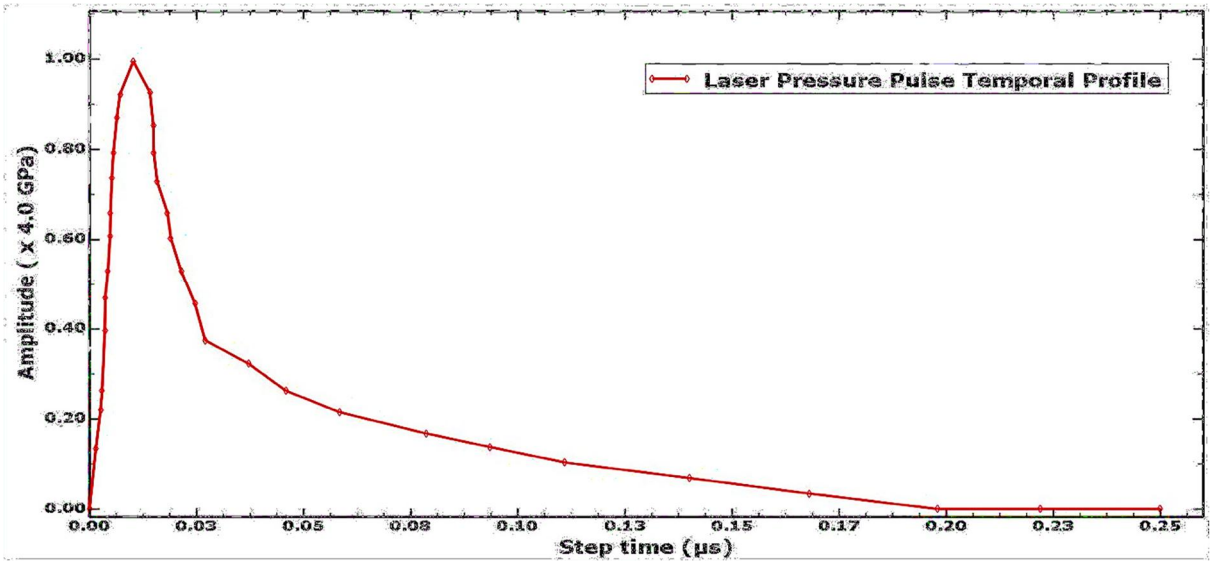


Figure 5: Temporal Loading Profile for the Simulation of LSP Loading Step [23]

The spatial distribution of the laser loads is designated as shots of circular geometry, corresponding to the spatial distribution of the pressure profile which for the purpose of this investigation has been adapted to be of Gaussian distribution where the laser power density is reckoned to be uniform across the area of the beam spot with a full width at half maximum (FWHM). The loading profiles were included on the Abaqus/CAE via load/amplitude sub-module detailing the variations of the load with time and space at each loading step. Table 4 provides information on the loading patterns employed in the simulation. The loading profiles where included on the Abaqus/CAE via the load.

Table 4: Specifications of the peening loads on the target material

| Laser Shot Parameters | Magnitude |
|---|---|
| Laser Power Intensity | 6 GW/cm$^2$ |
| Peak Pressure | 4 GPa (approx.) |
| Coverage | 20 spots/mm$^2$ |
| Spot diameter | 0.6 mm |
| % Overlap | 83.3% |
| Step Time | 250 ns |
| Stress Relaxation Time | 500 ns |
| Number of runs | 1 × 2 |
| Size of Workpiece | 20 mm × 20 mm × 10mm |

The presence of confining media (such as water) and ablative coatings contribute in immense measures to an increase in the intensity of shock waves transmitted through the target to produce compressive residual stresses. It is often a reasonable assumption that hydrostatic pressure implication on total stress is negligible for phenomena devoid of shock wave propagation [24]. The converse is the case for LSP processes with the nature of complex wave collisions and propagation inherent. Such assumptions do not hold in this instance. Laser–matter interaction in a confined regime models have been elaborated for estimating the induced pressure in that regime, which includes the hydrostatic pressure associated with the presence of a fluid medium within the domain of a fast-growing plasma. This hydrostatic pressure implication is due to the ultra-high strain rate complexion of LSP occasioned by presence of shock waves, and thus in this study has been imposed on the physical definition of the problem, as well as in its analysis. The hydrostatic pressure contribution to the overall pressure intensity during the shock loading described by the Mie-Gruneisen equation of state formulation is expressed mathematically by Equation 10 [22];

$$P = \frac{\rho_0 C_0^2 (\eta-1)[\eta-\frac{\Gamma_0}{2}(\eta-1)]}{[\eta-S(\eta-1)]^2} + \Gamma_0 E \qquad (10)$$

where $C_0$ is the bulk speed of sound, $\Gamma_0$ is the Gruneisen gamma at the reference state, $S$ is a linear hugoniot slope coefficient which is equivalent to $\partial U_s / \partial U_p$ where $U_s$ is the shock wave velocity, $U_p$ is the particle velocity, and E is the internal energy per unit reference specific volume. Table 5 provides the linear shock equation of state parameters employed in this study for X12Cr steel material.

Table 5: Equation of State Parameters for X12Cr. [22]

| Parameter | Value |
|---|---|
| $C_0$ | 4.313 km/s |
| $\boldsymbol{\Gamma_0}$ | 1.4545 |
| $\boldsymbol{S}$ | 2.06 |

### *4.2 Boundary Conditions*

Real life implementation of LSP of components often necessitate the clamping of the workpiece on an operating platform moving relative to the laser beam assembly or vice versa. Having configured the shot pattern for the simulation as highlighted in Table 4, the degree of freedom of the peened material was constrained at the base edges by assigning encastre boundary conditions which fixes the freedom of the workpiece in all translational and rotational directions. This reduces the complexity of the analysis matrix of the problem and thereby limit solution errors. In this work, infinite boundary elements were employed to define the boundaries of the model and ensure full transmission of the stress waves in accordance to the acoustic impedance of infinite elements, which in turn ensures that reflecting stress waves do not destructively interfere with the intensity of shock waves generated from the laser shocks. The boundary conditions are configured to be active at the analysis initialization phase and propagated through all the analysis steps, thereby forestalling boundary induced nonlinearities in the simulation, ensuring full shock energy recast to plasma pressure pulse formation without giving rise to global displacement of the geometry.

### *4.3 Mesh Selection and Design*

Design of the discretization of the geometry of the model was done in two domains, with deliberate consideration for features such as the selected analysis algorithm, the nature of physics of shock waves dissemination and loading type. A coupling of finite and the infinite elements domains were therefore employed. The laser shock impacted affected zone and its surroundings where discretized with a C3D8R mesh – 8-node first order linear brick hexahedral continuum finite elements with reduced integration and hour glass control mesh – with the peened regions modelled with a finer mesh with advancing bias around the region of intended depth of concentration of compressive residual stresses as shown in Figure 6. This process creates more analysis integration points around and through the thickness of the area of focus to obtain a better degree of accuracy in the stress and strain responses, since the output results at these points are the most important result to be obtained from the developed numerical model.

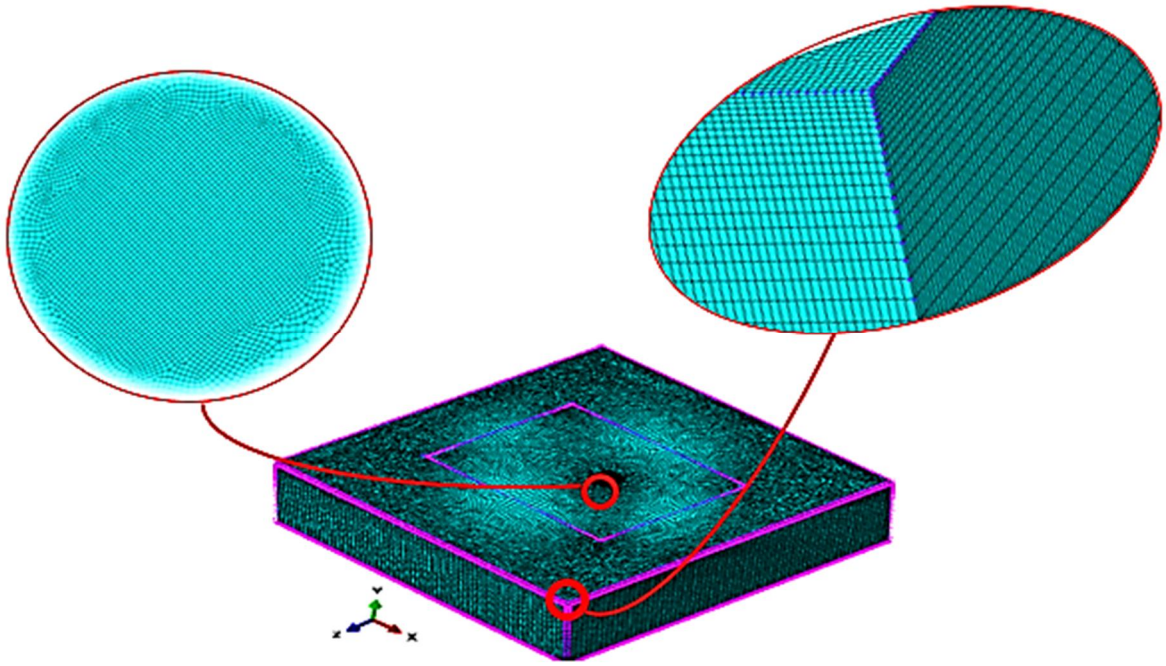

Figure 6: 3D discretized finite elements mesh model of the X12Cr block showing mesh refinement at areas of interest.

The outer boundaries of the model were adjoined with CIN3D8 – 8-node continuum linear infinite elements to simulate the in-plane transmission of shock waves from the shock affected zones (SAZ). The behaviour of shockwaves within the material during the duration of the aftershocks is often conflicted between complete reflection and complete transmission, and the quicker the system can be brought to as state of equilibrium, the faster the simulation and computational process. As stated earlier, reflecting stress waves interfere with intensity of generated shock waves and by extension the morphology of the deposition of the residual stresses. As shown in Figure 7, the infinite element boundaries provide acoustically quiet, non-reflecting boundaries which minimise the reflection of waves back into the SAZ. Furthermore, an extended finite element mesh domain was provided for the SAZ to ensure that a sufficient residual stress transmission and deposition field is available, without traversing the finite-infinite elements fringes, since the infinite boundary elements assume an elastic nature and hence would not react plastically to residual stress waves transmitted through it. The arrangement thus provides an outlet for shock waves propagating from the impact zone outwards from within the material. Since the accuracy of results frequently are hinged upon the type, size or distribution of mesh elements employed in a model, mesh convergence checks were implemented at the locations of interest which is at the region of the laser beam spot. This guarantees integrity of the results as well as maintaining a balance between the computational cost, period and element size. A mesh element size of 0.08 mm was thereafter selected, based on the outcomes of the mesh convergence checks, as the most suitable and computationally economical choice.

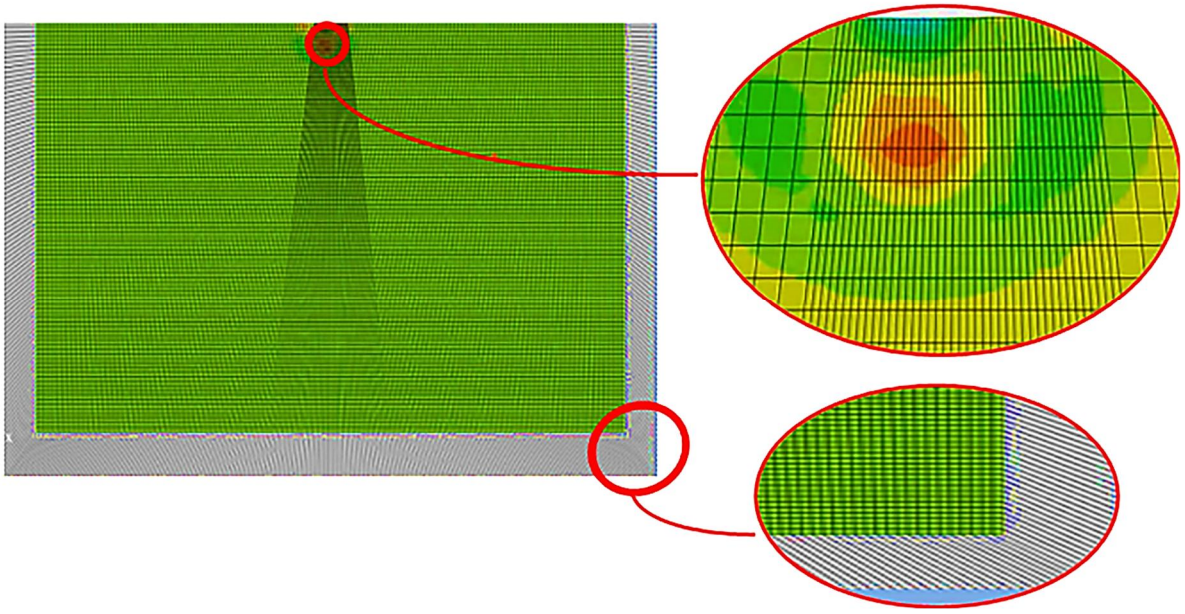

Figure 7: 2-D mesh section of the model showing the infinite boundary elements and mesh refinement around the SAZ

## 5. RESULTS AND DISCUSSION

Indispensably, the results of the simulation have been validated by experiments conducted with the peening parameters used in the numerical analysis. Samples of X12Cr steel blocks were machined from an out-of-service last stage low-pressure turbine blade obtained from a power station and heat treated to remove and residual stresses inherent from its manufacture and the machining process that produced the blocks. A commercial Nd:YAG laser operating at a wavelength of 1064nm was used to shock-peen the steel blocks. X-ray diffraction (XRD) technique was utilized to determine the profile and distribution of the residual stresses posited in the blocks after peening.

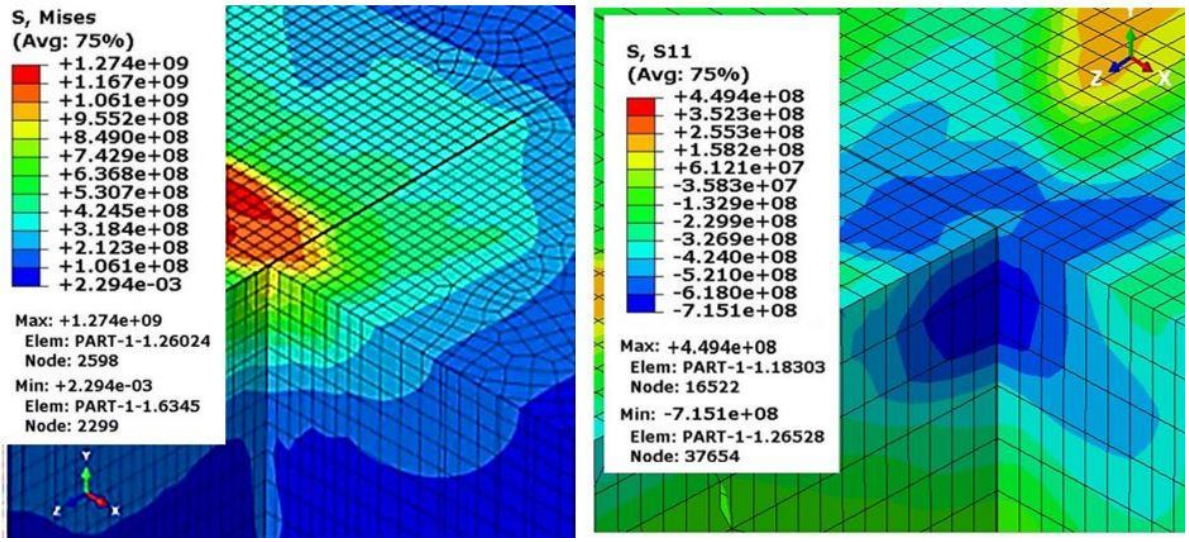


(a) (b)

Figure 8: Stress distribution results in a section of the simulation model

A 3D visualization of the stress distribution results in a section of the simulation model after the complete simulation using the coupled explicit-damping procedure are shown in Figure 8**.** The compressive residual stress field was analysed and validated along two sections, the transverse x-axis (for the surfaces residual stresses) and the longitudinal y-axis (for the plastically affected depth of compressive residual stresses) relative to Figure 8.The results of the simulation were extracted and benchmarked against those obtained from the experiments. Figure 9 shows a plot of the residual stresses against the depth of the plastically affected domain. The major economic parameters of concern in every laser shock peening operation are the residual stresses at the surface of the peened material (SRS), the maximum compressive residual stresses (MCRS), the depth of the maximum residual stresses (DMCRS) and the plastically affected depth of compressive residual stresses (MDCRS).

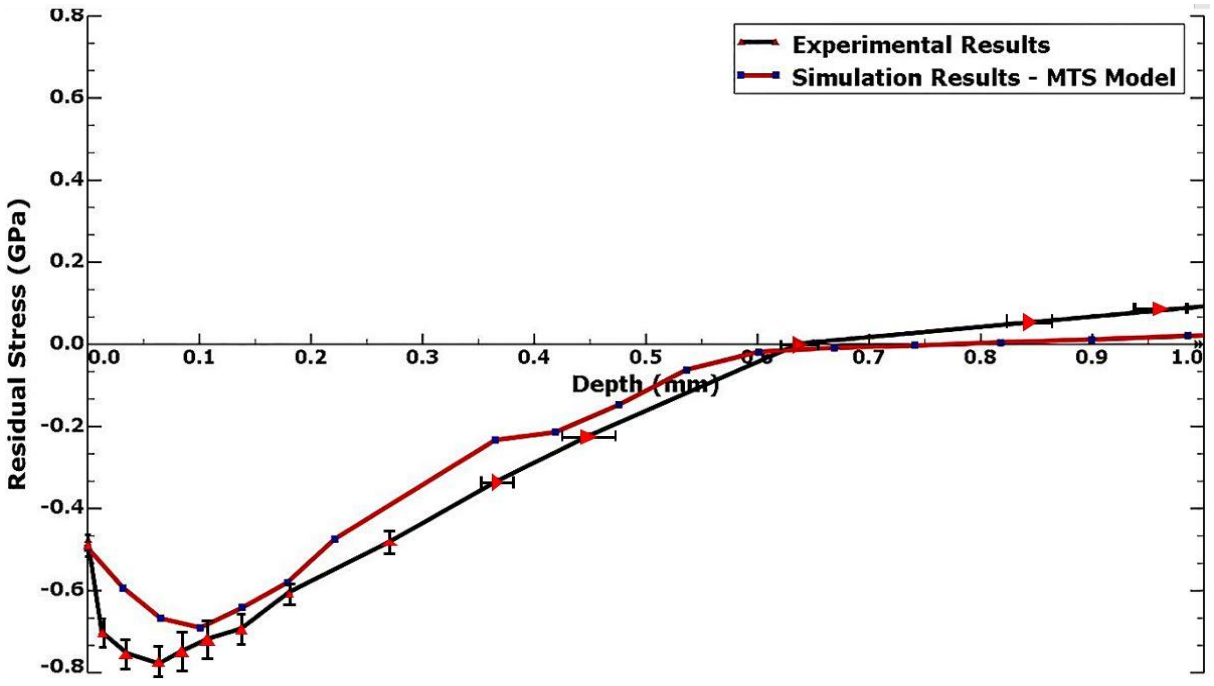


Figure 9: Superimposed Simulated and Experimental Residual Stresses against Depth

From Figure 9, the simulated stresses have been compared to those obtained from the experiment, comparing the S11 results vs affected depth for the 4 major economic parameters earlier stated. The results and comparisons are highlighted in table 6 showing the close correlations obtained from the constitutive model and analysis procedure employed in the simulation of the LSP process.

Table 6: Comparisons of Experimental and Simulated Results of the LSP process

| Parameter Description | Experiment | Simulation | Comments/ Inference |
|---|---|---|---|
| Surface Residual Stress [SRS] (GPa) | -0.46 | -0.48 | Close correlation (3.6% variation). |
| Maximum Compressive Residual Stress [MCRS] (GPa) | -0.77 | -0.715 | Close correlation (7.1% variation). |
| Depth of MCRS (mm) | 0.064 | 0.10 | MCRS observed to occur deeper in the material. |
| Maximum depth of CRS (mm) | 0.64 | 0.67 | CRS observed to occur deeper in the material. (4.5% variation). |

Despite slight variations from the experimental data, the overall trend and profiles of the residual stresses' domain was captured accurately by the simulation, thereby validating the developed numerical model. The slight variations may be attributed to simulation assumptions such as the influence of exact temporal profile of the pressure pulse obtained during LSP and the multi-shot simulation pattern which are currently still a subject of academic investigation. Comparative analysis of experimental and numerical simulation results thus gives confidence and validity to the adoption of the MTS material model as a one that is applicable for simulating laser shock peening.

***Impacted Depth Threshold***

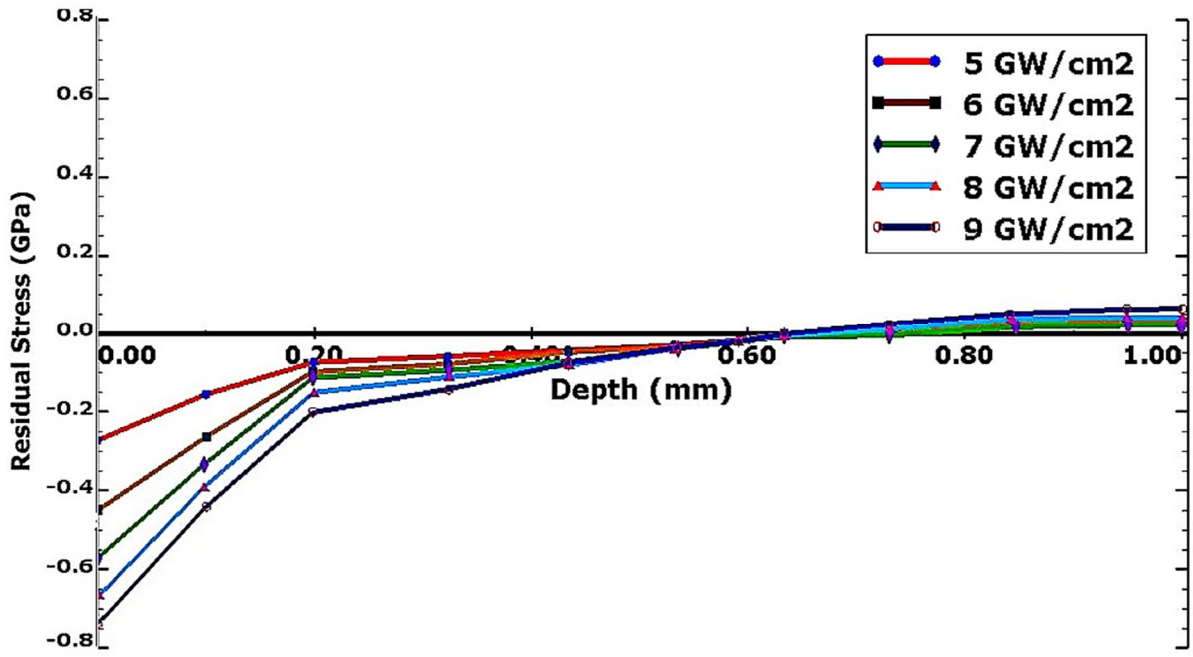


Figure 10: Impacted Depth Analysis for Graduated Shot Intensities.

From Equation 8, it is given that the peak pressure of laser shockwaves is proportional to the square root of the intensity of the laser load. Using the MTS constitutive model, the effect of increased loading was investigated and revealed progressive increases in the surface residual stresses, increasing in proportion with increased shock load intensity. However, as shown in Figure 10 the depth of penetration is retained at a threshold, at approximately 0.6 mm where progressive increase in the magnitude of shock loading does not translate to increased maximum depth of compressive residual stresses (MDCRS). This is contrary to the impression provided with empirical models, that tends to suggest on proportional increase in MDCRS with progressive amplification of the laser shock load intensity. Interestingly, this too has been overlooked by researchers as the primary interest has always been the economic importance of induction of surface residual stresses which laser shock peening as a technique offers. This impacted depth threshold is further explained by the dislocation motion during impact induced deformation of materials. The continual fluctuations in the stress field within the material reaches a crescendo wherein the lattice of the material have been rearranged into a cluster of dislocating crystal lattice grains leading to an increase in the yield strength, fatigue and crack formation resistance of the material. There however exists a threshold where a dislocation filled domain hinders further dislocations, plastic deformations or induction of compressive residual stresses. The results of modelling with the MTS model thus helps in determining this threshold depth beyond which no further plastic deformation or induction of compressive stresses can be attained by mere accumulation of dislocations occasioned by the laser shock wave pressure within a material. This provides useful guidance for practical control of the LSP operation in terms of excessive peening of a material beyond what should have been their threshold limits to the point where the material's mechanical property is closer to fracture, rather than preventing it from fracture.

## 6. CONCLUSION

This study has presented an alternate computational modelling and simulation of laser shock peening on X12Cr steel using an alternate computational mechanical threshold plasticity model which is founded on a physics-based formulation that describes a mechanical threshold for compressive residual stress induction irrespective of increasing shock intensities. The use of LSP for improving the surface and internal compressive stress fields of components like turbine blades, which research and experience have proven to be susceptible to failure by fatigue and crack initiated damages, is very much desirable. However, as stated in some previously published reviews, the desire to achieve supreme magnitudes of CRS and uttermost depths of induced stresses has the tendency to lead to internal ruptures due to 'over-processing'. This practise is borne, as indicated by [14], out of impressions which tend to suggest that a material can be infinitely induced with CRS to infinite depths by simply ramping up laser shock intensities. The phenomenon of mechanical thresholds of plastically affected depths during LSP is one which hitherto has previously been overlooked by many researchers, but which has been investigated in this study and the results, validated experimentally. Based on the foregoing, the model used in the finite element simulation of LSP in this study, which has been supported by experimental study, has described with a great deal of accuracy the outcomes of LSP on engineering materials and thus can be applicable as a faster and cost saving alternative for further investigative studies on LSP. The Mechanical Threshold Stress (MTS) constitutive model, a model which takes into account the graduation of hardening from stage to stage during ultra-high strain rate shock processing and strain-hardening induced dislocation accumulation and annihilation, provides a reliable formulation for describing, analysing and predicting shock response of X12Cr material to laser shock loading. Having applied a mechanical threshold plasticity model, which has shown that there exists a depth of penetration retained at a threshold where progressive increases in the magnitude of shock loading does not translate to increased maximum depth of compressive residual stresses, the knowledge of the threshold depth of materials can help ease concerns on appropriate parameters for treating them with the LSP technique, especially with specialized non-uniform geometries such as aerofoils. Internal defects and ruptures resulting from over-peening of critical components can also be avoided.

## ACKNOWLEDGEMENTS

The authors wish to acknowledge the financial and technical support of the National Research Foundation (NRF Grant Reference No: SFH170720255948), Eskom, the National Laser Centre, Centre for Scientific an Industrial Research, Pretoria , Tshwane University of Technology and the Department of Science and Technology, Republic of South Africa towards the success of this research. Opinions expressed and conclusions arrived at are those of the author(s) and are not necessarily to be attributed to the NRF.

## REFERENCES

1. Cleland, John. 2013. World Population Growth; Past, Present and Future. Environmental and Resource Economics. 55. 10.1007/s10640-013-9675-6.
2. IEA 2019. "World Energy Outlook 2019", IEA, Paris https://www.iea.org/reports/world-energy-outlook-2019. (Accessed 14 July 2020).
3. Ziegler D 2013 Investigation of turbine blade failure in a thermal power plant. Case Studies in Engineering Failure Analysis. Elsevier Ltd., vol. 1(3), 192–199.
4. Ran, Z et al. 2018. Finite Element Analysis of Surface Roughness Generated by Multiple Laser Shock Peening. Rare Metal Materials and Engineering Journal, 47(1): 0033-0038. DOI:10.1016/S1875-5372(18)30067-5
5. Pretorius, J. G., Desai, D. A., & Snedden, G. C. 2019. Effect of laser shock peening on fatigue life at stress raiser regions of a high-speed micro gas turbine shaft: A simulation-based study. International Journal of Engineering Research in Africa, *45*, 15–27. https://doi.org/10.4028/www.scientific.net/JERA.45.15
6. Braisted, W., & Brockman, R. 1999. Finite element simulation of laser shock peening. International Journal of Fatigue, Elsevier Science Ltd *21*, 719–724.
7. Karbalaian, H. R. et al. 2015. Investigation on the Effect of Overlapping Laser Pulses in Laser Shock Peening with Finite Element Method. Procedia Materials Science. Elsevier B.V., 11, pp. 454–458. doi: 10.1016/j.mspro.2015.11.045
8. Peyre, P., Fabbro, R., Berthe, L. & Dubouchet, C. 1996. Laser shock processing of materials, physical processes involved and examples of applications. Journal of Laser Applications, vol.8, pp. 135-141.
9. Ran, Z et al. 2018. Finite Element Analysis of Surface Roughness Generated by Multiple Laser Shock Peening. Rare Metal Materials and Engineering Journal, 47(1): 0033-0038. doi:10.1016/S1875-5372(18)30067-5
10. Vasu, A., Gobal, K. & Grandhi, R. V. 2015. A computational methodology for determining the optimum re-peening schedule to increase the fatigue life of laser peened aircraft components. International Journal of Fatigue. Elsevier Ltd, 70, pp. 395–405.
11. Wang, C. et al. 2016. Numerical modelling of the confined laser shock peening of the OFHC copper. International Journal of Mechanical Sciences. Elsevier, vol.108, pp. 104–114.
12. Zhou, Z. et al. 2011. A finite element study of thermal relaxation of residual stress in laser shock peened IN718 superalloy. Intl. Journal of Impact Engineering. Elsevier Ltd, 38(7), pp. 590–596.
13. Peyre, P. 2017. Laser Shock Processing on Metal. Metals, 7(10), 409. https://doi.org/10.3390/met7100409
14. Rockstroh, T.J.; Bailey, M.S.; Ash, C.A.; Ulanski, W. 2008 Laser Shock Processing of Aircraft Engine Components; General Electric Infrastructure-Aviation: Cincinnati, OH, USA.
15. Jansen van Rensburg, G. J. & Kok, S. 2012. Tutorial on state variable based plasticity: An Abaqus UHARD subroutine. Eighth South African Conference on Computational and Applied Mechanics,158–165.

16. Kok, S., Beaudoin, A. J., & Tortorelli, D. A. 2002. A polycrystal plasticity model based on the mechanical threshold. International Journal of Plasticity, 18(5–6), 715–741. https://doi.org/10.1016/S0749-6419(01)00051-1
17. Peyre, P., Berthe, L., & Popa, I. 2012. Analysis of laser shock waves and resulting surface deformations in an Al – Cu – Li aluminium alloy. March 2015. https://doi.org/10.1088/0022-3727/45/33/335304
18. Banerjee B. 2007. The Mechanical Threshold Stress Model for Various Tempers of AISI 4340 Steel. International Journal of Solids and Structures., 44(3), 834–859. https://doi.org/10.1016/j.ijsolstr.2006.05.022
19. Kok, S., Beaudoin, A. J., & Tortorelli, D. A. 2002. On the development of stage IV hardening using a model based on the mechanical threshold. Acta Materialia, *50*(7), 1653–1667. https://doi.org/10.1016/S1359-6454(02)00002-2
20. Jansen Van Rensburg, G. J., Kok, S., & Wilke, D. N. 2016. Cyclic effects and recrystallisation in temperature and rate dependent state variable based plasticity. Proceedings of the 10th South African Conference on Computational and Applied Mechanics, SACAM 2016, October
21. Kuveya, K. R., Polese, C., & Newby, M. 2016. Laser Peening versus Shot Peening Effects on Residual Stress and Surface Modification of X12CrNiMo12 Turbine Blade. 6th International Conference on Laser Peening and Related Phenomena, (November), 6–11.
22. Armfield, D. 2018. Optimised Implementation of Physics-based Strain-rate Dependent Material Models for the Improved Simulation of the Laser Shock Peening Process. University of Pretoria.
23. Hfaiedh, N. et al. 2015. Finite element analysis of laser shock peening of 2050-T8 aluminum alloy, International Journal of Fatigue. Elsevier Ltd, 70, pp. 480–489. doi: 10.1016/j.ijfatigue.2014.05.015.
24. Hiermaier, S. J. 2008. Structures under crash and impact: Continuum mechanics, discretization and experimental characterization 1–410. doi:10.1007/978-0-387-73863-5